Supplemental Information for 'Pressure-dependent kinetics of isobutanol peroxy isomers'

Mark Jacob Goldman†, Nathan Wa-Wai Lee†, Jesse H. Kroll† & William H. Green†

July 23, 2020

† Department of Chemical Engineering, Massachusetts Institute of Technology, 77 Massachusetts Avenue, Cambridge, MA 02139, USA

Overview of Supplemental Information

S1 Contains the product branching when changing barrier heights, collision rate, and the method of obtaining k(T,P)

S2 Contains the range of values of branching ratios and overall reactions rates from the Monte carlo simulations

S3 Contains videos of each reaction's internal reaction coordinate calculation

S4 Contains figures not described in the above categories

S1 Product branching sensitivity analysis

This section contains figures of the product branching when changing barrier heights, collision rate, and the method of obtaining k(T,P).

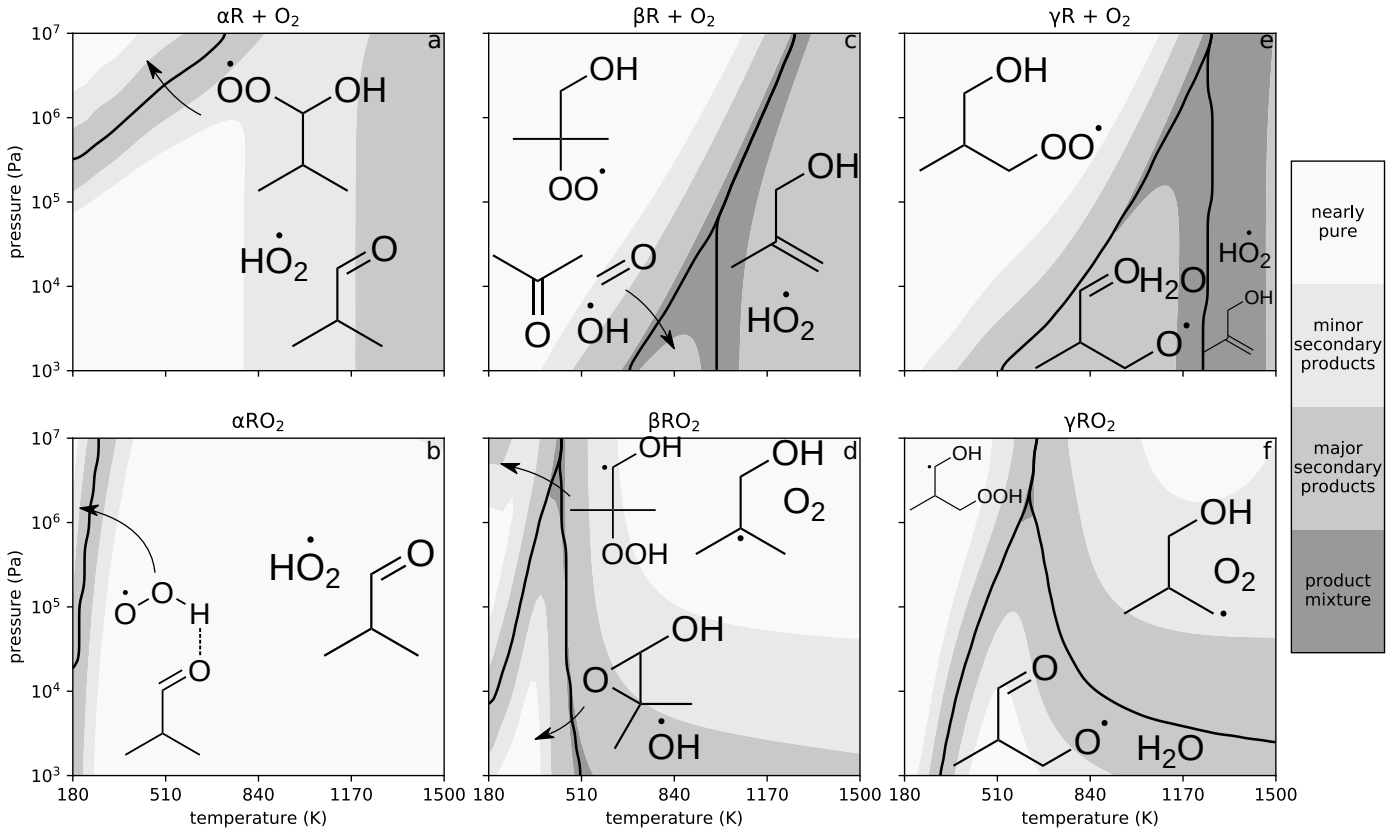

Figure S1: To observe sensitivity to barrier hights, **αAdductFromRO2** was increased by 13 kJ/mol, **β-γHO2elimFromRO2** was increased by 10 kJ/mol (corresponding to the barrier height in Sun et al.), and **γH2OForm** was decreased by 6 kJ/mol (corresponding to the barrier height in Welz et al.). The major products formed and branching ratio of alkyl + O_2 reactions and peroxy reactions for the α, β, and γ networks at various temperatures and pressures. The structures indicate the major product from the reaction. Shading indicates the fraction going to the major pathway indicated, with cutoffs at 90%, 75%, and 40%. Text gives a qualitative description to the different colors.

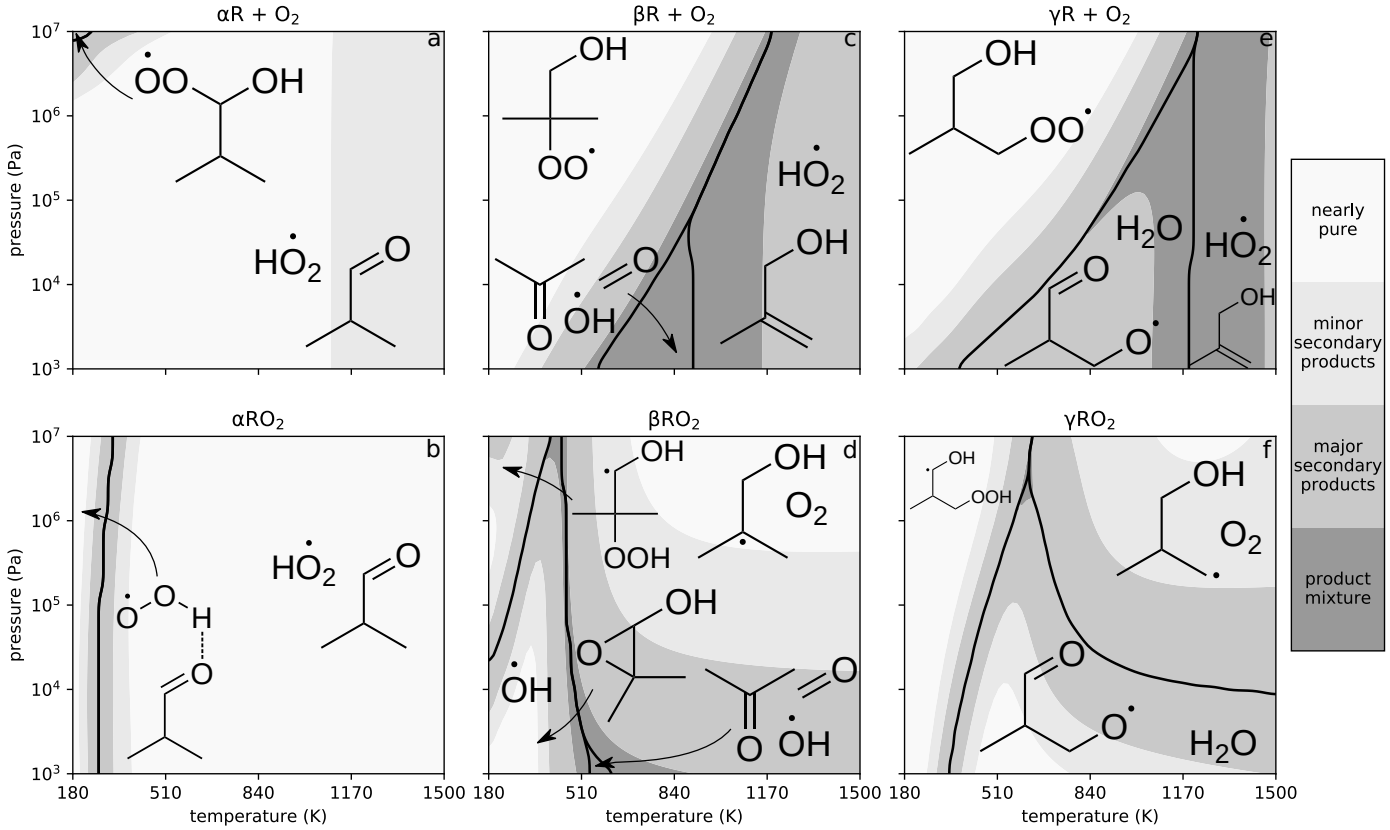

Figure S2: To observe sensitivity to the collisional energy, the collisional energy transfer of all isomers was decreased by a factor of two. The major products formed and branching ratio of alkyl + O_2 reactions and peroxy reactions for the α, β, and γ networks at various temperatures and pressures. The structures indicate the major product from the reaction. Shading indicates the fraction going to the major pathway indicated, with cutoffs at 90%, 75%, and 40%. Text gives a qualitative description to the different colors.

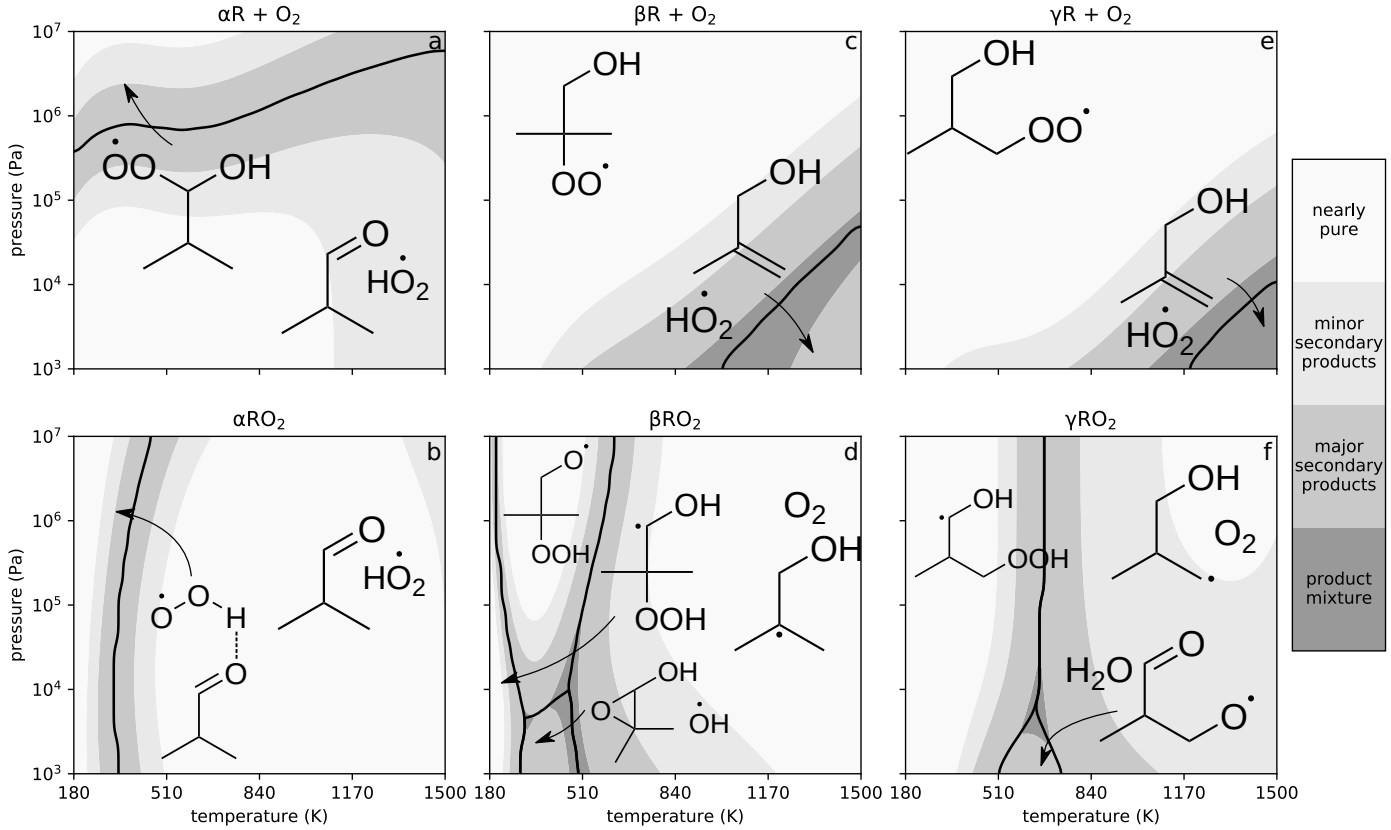

Figure S3: To observe sensitivity to the method used, modified strong collision approximation was used instead of reservoir state approximation. The major products formed and branching ratio of alkyl + O_2 reactions and peroxy reactions for the α, β, and γ networks at various temperatures and pressures. The structures indicate the major product from the reaction. Shading indicates the fraction going to the major pathway indicated, with cutoffs at 90%, 75%, and 40%. Text gives a qualitative description to the different colors.

S2 Branching ratio confidence intervals

Using the Monte carlo generated networks, uncertainty on the branching ratios (Tables S1-S18) and on the overall rates (Tables S19-S21) for the reaction between $R + O_2$ and unimolecular RO_2 radicals.

For these runs, the varied energy levels of stationary points (E_0), rates of reactions used in inverse Laplace transform (r_{A+B}), the exponent in the energy transfer expression ($\langle E_{down} \rangle = A \times (T/300K)^{\mathbf{n}}$), and the method used to solve for phenomenological rate constants (reservoir state or modified strong collision) showed up as important factors in the uncertainty of branching ratios and/or overall reaction rates, based on the Spearman rank correlation value, τ.

Table S1: Branching ratio uncertainty for αR + O2 at 300 K and 1×10^5 Pa. The median and 90% confidence interval of the branching ratio for each pathway are shown using data from Monte carlo simulations. For each branch point, the two parameters with the highest correlation, τ, determined using the Spearman rank correlation, are shown with their corresponding values. See S2 for description of the parameter names.

path	5%	50%	95%	factor	τ	factor	τ
O2 + αR $\rightleftharpoons$ HO2 + isobutanal	0.387	0.990	1.000	αAdductFromRO2 E_0	-0.547	reservoir state	0.453
O2 + αR $\rightleftharpoons$ αRO2	2×10^{-12}	0.003	0.558	αAdductFromRO2 E_0	0.519	reservoir state	-0.460
O2 + αR $\rightleftharpoons$ ipropyl + performic_acid	5×10^{-5}	0.001	0.017	α-βscissionFromAlkoxy E_0	-0.619	αAdductFromRO2 E_0	0.509

Table S2: Branching ratio uncertainty for αR + O2 at 600 K and 3×10^5 Pa. The median and 90% confidence interval of the branching ratio for each pathway are shown using data from Monte carlo simulations. For each branch point, the two parameters with the highest correlation, τ, determined using the Spearman rank correlation, are shown with their corresponding values. See S2 for description of the parameter names.

path	5%	50%	95%	factor	τ	factor	τ
O2 + αR $\rightleftharpoons$ HO2 + isobutanal	0.356	0.971	0.999	reservoir state	0.518	αAdductFromRO2 E_0	-0.513
O2 + αR $\rightleftharpoons$ αRO2	1×10^{-11}	0.002	0.560	reservoir state	-0.539	αAdductFromRO2 E_0	0.450
O2 + αR $\rightleftharpoons$ ipropyl + performic_acid	9×10^{-4}	0.007	0.063	α-βscissionFromAlkoxy E_0	-0.575	αAdductFromRO2 E_0	0.548
O2 + αR $\rightleftharpoons$ αadduct	1×10^{-15}	7×10^{-8}	0.011	reservoir state	-0.426	$r_{isobutanal+HO2}$	-0.375

Table S3: Branching ratio uncertainty for αR + O2 at 900 K and 1×10^6 Pa. The median and 90% confidence interval of the branching ratio for each pathway are shown using data from Monte carlo simulations. For each branch point, the two parameters with the highest correlation, τ, determined using the Spearman rank correlation, are shown with their corresponding values. See S2 for description of the parameter names.

path	5%	50%	95%	factor	τ	factor	τ
O2 + αR $\rightleftharpoons$ HO2 + isobutanal	0.275	0.940	0.992	reservoir state	0.564	αAdductFromRO2 E_0	-0.467
O2 + αR $\rightleftharpoons$ αRO2	4×10^{-12}	4×10^{-4}	0.653	reservoir state	-0.601	αAdductFromRO2 E_0	0.404
O2 + αR $\rightleftharpoons$ ipropyl + performic_acid	0.005	0.029	0.165	α-βscissionFromAlkoxy E_0	-0.533	αAdductFromRO2 E_0	0.533
O2 + αR $\rightleftharpoons$ αadduct	2×10^{-16}	3×10^{-9}	0.012	reservoir state	-0.519	$r_{isobutanal+HO2}$	-0.327

Table S4: Branching ratio uncertainty for αRO2 at 300 K and 1×10^5 Pa. The median and 90% confidence interval of the branching ratio for each pathway are shown using data from Monte carlo simulations. For each branch point, the two parameters with the highest correlation, τ, determined using the Spearman rank correlation, are shown with their corresponding values. See S2 for description of the parameter names.

path	5%	50%	95%	factor	τ	factor	τ
αRO2 $\rightleftharpoons$ HO2 + isobutanal	9×10^{-4}	0.549	1.000	isobutanal E_0	-0.591	αadduct E_0	0.386
αadduct $\rightleftharpoons$ αRO2	3×10^{-4}	0.453	0.999	isobutanal E_0	0.591	αadduct E_0	-0.385

Table S5: Branching ratio uncertainty for αRO2 at 600 K and 3×10^5 Pa. The median and 90% confidence interval of the branching ratio for each pathway are shown using data from Monte carlo simulations. For each branch point, the two parameters with the highest correlation, τ, determined using the Spearman rank correlation, are shown with their corresponding values. See S2 for description of the parameter names.

path	5%	50%	95%	factor	τ	factor	τ
αRO2 $\rightleftharpoons$ HO2 + isobutanal	0.433	0.997	1.000	αadduct E_0	0.440	isobutanal E_0	-0.355
αadduct $\rightleftharpoons$ αRO2	7×10^{-8}	0.002	0.568	αadduct E_0	-0.459	isobutanal E_0	0.400

Table S6: Branching ratio uncertainty for αRO2 at 900 K and 1×10^6 Pa. The median and 90% confidence interval of the branching ratio for each pathway are shown using data from Monte carlo simulations. For each branch point, the two parameters with the highest correlation, τ, determined using the Spearman rank correlation, are shown with their corresponding values. See S2 for description of the parameter names.

path	5%	50%	95%	factor	τ	factor	τ
αRO2 $\rightleftharpoons$ HO2 + isobutanal	0.678	0.998	1.000	αAdductFromRO2 E_0	-0.476	reservoir state	0.435
αadduct $\rightleftharpoons$ αRO2	2×10^{-10}	1×10^{-5}	0.172	αadduct E_0	-0.449	reservoir state	-0.437
O2 + αR $\rightleftharpoons$ αRO2	3×10^{-12}	8×10^{-6}	0.086	$r_{\alpha R+O_2}$	0.651	αAdductFromRO2 E_0	0.412
αRO2 $\rightleftharpoons$ ipropyl + performic_acid	2×10^{-7}	5×10^{-4}	0.028	αAdductFromRO2 E_0	0.660	reservoir state	-0.325

Table S7: Branching ratio uncertainty for βR + O2 at 300 K and 1×10^5 Pa. The median and 90% confidence interval of the branching ratio for each pathway are shown using data from Monte carlo simulations. For each branch point, the two parameters with the highest correlation, τ, determined using the Spearman rank correlation, are shown with their corresponding values. See S2 for description of the parameter names.

path	5%	50%	95%	factor	τ	factor	τ
O2 + βR ⇌ βRO2	0.955	0.998	1.000	βRO2 E_0	-0.573	βR E_0	-0.402
O2 + βR ⇌ OH + trisub_epoxy	2×10^{-6}	2×10^{-4}	0.011	β-αQOOHIsom E_0	-0.705	βRO2 E_0	0.423

Table S8: Branching ratio uncertainty for βR + O2 at 600 K and 3×10^5 Pa. The median and 90% confidence interval of the branching ratio for each pathway are shown using data from Monte carlo simulations. For each branch point, the two parameters with the highest correlation, τ, determined using the Spearman rank correlation, are shown with their corresponding values. See S2 for description of the parameter names.

path	5%	50%	95%	factor	τ	factor	τ
O2 + βR ⇌ βRO2	0.786	0.982	0.999	$r_{\beta R+O_2}$	0.477	βRO2 E_0	-0.445
O2 + βR ⇌ HO2 + ibutenol	6×10^{-5}	0.003	0.069	β-αHO2elimFromRO2 E_0	-0.619	$r_{\beta R+O_2}$	-0.458
O2 + βR ⇌ HO2 + γalkene	6×10^{-5}	0.003	0.059	β-γHO2elimFromRO2 E_0	-0.624	$r_{\beta R+O_2}$	-0.490
O2 + βR ⇌ OH + trisub_epoxy	4×10^{-5}	0.001	0.034	β-αQOOHIsom E_0	-0.638	$r_{\beta R+O_2}$	-0.358
O2 + βR ⇌ CH2O + OH + acetone	8×10^{-5}	0.003	0.046	$r_{\beta R+O_2}$	-0.391	βDoubleβscission E_0	-0.389

Table S9: Branching ratio uncertainty for βR + O2 at 900 K and 1×10^6 Pa. The median and 90% confidence interval of the branching ratio for each pathway are shown using data from Monte carlo simulations. For each branch point, the two parameters with the highest correlation, τ, determined using the Spearman rank correlation, are shown with their corresponding values. See S2 for description of the parameter names.

path	5%	50%	95%	factor	τ	factor	τ
O2 + βR ⇌ βRO2	0.292	0.922	0.997	reservoir state	-0.573	βRO2 E_0	-0.477
O2 + βR ⇌ HO2 + ibutenol	6×10^{-4}	0.020	0.279	β-αHO2elimFromRO2 E_0	-0.539	reservoir state	0.507
O2 + βR ⇌ HO2 + γalkene	6×10^{-4}	0.019	0.265	β-γHO2elimFromRO2 E_0	-0.517	reservoir state	0.490
O2 + βR ⇌ CH2O + OH + acetone	2×10^{-4}	0.009	0.117	reservoir state	0.637	βRO2 E_0	0.412
O2 + βR ⇌ OH + trisub_epoxy	1×10^{-4}	0.005	0.123	β-αQOOHIsom E_0	-0.535	reservoir state	0.529

Table S10: Branching ratio uncertainty for βRO2 at 300 K and 1×10^5 Pa. The median and 90% confidence interval of the branching ratio for each pathway are shown using data from Monte carlo simulations. For each branch point, the two parameters with the highest correlation, τ, determined using the Spearman rank correlation, are shown with their corresponding values. See S2 for description of the parameter names.

path	5%	50%	95%	factor	τ	factor	τ
βQOOH[O] ⇌ βRO2	3×10^{-5}	0.112	0.998	βQOOH[O] E_0	-0.562	β-αQOOHIsom E_0	0.471
βQOOHα ⇌ βRO2	1×10^{-7}	0.068	0.982	β-αQOOHIsom E_0	-0.469	imaginary freq. β-αQOOHIsom	0.453
βRO2 ⇌ OH + trisub_epoxy	1×10^{-5}	0.037	0.902	β-αQOOHIsom E_0	-0.442	βEpoxyFromα E_0	-0.374
βRO2 ⇌ CH2O + OH + acetone	7×10^{-8}	3×10^{-4}	0.522	βDoubleβscission E_0	-0.754	β-αQOOHIsom E_0	0.331
O2 + βR ⇌ βRO2	2×10^{-10}	6×10^{-6}	0.295	$r_{\beta R+O_2}$	0.665	βR E_0	-0.568
βRO2 ⇌ HO2 + γalkene	7×10^{-8}	2×10^{-4}	0.207	β-γHO2elimFromRO2 E_0	-0.724	β-αQOOHIsom E_0	0.344
βRO2 ⇌ HO2 + ibutenol	2×10^{-7}	1×10^{-4}	0.060	β-αHO2elimFromRO2 E_0	-0.543	βHO2elimFromα E_0	-0.288
βQOOHγ ⇌ βRO2	6×10^{-10}	4×10^{-6}	0.032	β-γQOOHIsom E_0	-0.574	imaginary freq. β-γQOOHIsom	0.560

Table S11: Branching ratio uncertainty for βRO2 at 600 K and 3×10^5 Pa. The median and 90% confidence interval of the branching ratio for each pathway are shown using data from Monte carlo simulations. For each branch point, the two parameters with the highest correlation, τ, determined using the Spearman rank correlation, are shown with their corresponding values. See S2 for description of the parameter names.

path	5%	50%	95%	factor	τ	factor	τ
O2 + βR ⇌ βRO2	3×10^{-4}	0.489	0.998	$r_{\beta R+O_2}$	0.862	βR E_0	-0.396
βRO2 ⇌ OH + trisub_epoxy	4×10^{-5}	0.021	0.662	β-αQOOHIsom E_0	-0.578	$r_{\beta R+O_2}$	-0.564
βRO2 ⇌ CH2O + OH + acetone	5×10^{-5}	0.027	0.624	$r_{\beta R+O_2}$	-0.603	βDoubleβscission E_0	-0.492
βRO2 ⇌ HO2 + γalkene	3×10^{-5}	0.015	0.576	$r_{\beta R+O_2}$	-0.632	β-γHO2elimFromRO2 E_0	-0.593
βRO2 ⇌ HO2 + ibutenol	2×10^{-5}	0.014	0.471	$r_{\beta R+O_2}$	-0.623	β-αHO2elimFromRO2 E_0	-0.539
βQOOH[O] ⇌ βRO2	7×10^{-9}	5×10^{-6}	0.514	reservoir state	-0.702	βQOOH[O] E_0	-0.405
βQOOHα ⇌ βRO2	8×10^{-12}	6×10^{-5}	0.072	reservoir state	-0.500	βEpoxyFromα E_0	0.430

Table S12: Branching ratio uncertainty for βRO2 at 900 K and 1×10^6 Pa. The median and 90% confidence interval of the branching ratio for each pathway are shown using data from Monte carlo simulations. For each branch point, the two parameters with the highest correlation, τ, determined using the Spearman rank correlation, are shown with their corresponding values. See S2 for description of the parameter names.

path	5%	50%	95%	factor	τ	factor	τ
O2 + βR ⇌ βRO2	0.003	0.879	1.000	$r_{\beta R+O_2}$	0.915	βR E_0	-0.314
βRO2 ⇌ HO2 + γalkene	2×10^{-5}	0.017	0.535	$r_{\beta R+O_2}$	-0.831	β-γHO2elimFromRO2 E_0	-0.430
βRO2 ⇌ HO2 + ibutenol	1×10^{-5}	0.017	0.544	$r_{\beta R+O_2}$	-0.827	β-αHO2elimFromRO2 E_0	-0.400
βRO2 ⇌ CH2O + OH + acetone	2×10^{-5}	0.014	0.331	$r_{\beta R+O_2}$	-0.812	βR E_0	0.294
βRO2 ⇌ OH + trisub_epoxy	2×10^{-5}	0.008	0.258	$r_{\beta R+O_2}$	-0.764	β-αQOOHIsom E_0	-0.442
βQOOH[O] ⇌ βRO2	6×10^{-12}	2×10^{-9}	0.084	reservoir state	-0.737	βQOOH[O] E_0	-0.349
βQOOHα ⇌ βRO2	1×10^{-14}	1×10^{-7}	0.015	reservoir state	-0.688	βEpoxyFromα E_0	0.351

Table S13: Branching ratio uncertainty for γR + O2 at 300 K and 1×10^5 Pa. The median and 90% confidence interval of the branching ratio for each pathway are shown using data from Monte carlo simulations. For each branch point, the two parameters with the highest correlation, τ, determined using the Spearman rank correlation, are shown with their corresponding values. See S2 for description of the parameter names.

path	5%	50%	95%	factor	τ	factor	τ
O2 + γR ⇌ γRO2	0.930	0.998	1.000	γ-αQOOHIsom E_0	0.607	γRO2 E_0	-0.537
O2 + γR ⇌ H2O + γaldoxy	2×10^{-6}	3×10^{-4}	0.027	γ-αQOOHIsom E_0	-0.501	γRO2 E_0	0.392
O2 + γR ⇌ γQOOHα	1×10^{-7}	5×10^{-4}	0.024	γ-αQOOHIsom E_0	-0.506	γRO2 E_0	0.367

Table S14: Branching ratio uncertainty for γR + O2 at 600 K and 3×10^5 Pa. The median and 90% confidence interval of the branching ratio for each pathway are shown using data from Monte carlo simulations. For each branch point, the two parameters with the highest correlation, τ, determined using the Spearman rank correlation, are shown with their corresponding values. See S2 for description of the parameter names.

path	5%	50%	95%	factor	τ	factor	τ
O2 + γR ⇌ γRO2	0.845	0.991	0.999	γRO2 E_0	-0.461	γ-αQOOHIsom E_0	0.454
O2 + γR ⇌ H2O + γaldoxy	1×10^{-5}	0.002	0.079	reservoir state	0.589	γ-αQOOHIsom E_0	-0.417
O2 + γR ⇌ OH + disub_c4ether	3×10^{-6}	4×10^{-4}	0.026	reservoir state	0.510	γC4EtherFromα E_0	-0.418
O2 + γR ⇌ γQOOHα	2×10^{-9}	3×10^{-4}	0.021	γQOOHαE_0	-0.513	reservoir state	-0.332

Table S15: Branching ratio uncertainty for γR + O2 at 900 K and 1×10^{6} Pa. The median and 90% confidence interval of the branching ratio for each pathway are shown using data from Monte carlo simulations. For each branch point, the two parameters with the highest correlation, τ, determined using the Spearman rank correlation, are shown with their corresponding values. See S2 for description of the parameter names.

path	5%	50%	95%	factor	τ	factor	τ
O2 + γR ⇌ γRO2	0.265	0.958	0.998	reservoir state	-0.668	γRO2 E_0	-0.501
O2 + γR ⇌ H2O + γaldoxy	3×10^{-5}	0.009	0.378	reservoir state	0.733	γRO2 E_0	0.395
O2 + γR ⇌ OH + disub_c4ether	1×10^{-5}	0.004	0.165	reservoir state	0.705	γRO2 E_0	0.354
O2 + γR ⇌ HO2 + γalkene	1×10^{-4}	0.006	0.094	reservoir state	0.622	γHO2elimFromRO2 E_0	-0.477
O2 + γR ⇌ OH + disub_epoxy	3×10^{-5}	0.001	0.029	reservoir state	0.607	γ-βQOOHIsom E_0	-0.477
O2 + γR ⇌ CH2O + ipropylOOH	2×10^{-5}	9×10^{-4}	0.018	reservoir state	0.691	γRO2 E_0	0.416
O2 + γR ⇌ CH2O + OH + propene3ol	1×10^{-6}	4×10^{-4}	0.012	reservoir state	0.717	γDoubleβscissionFromγ E_0	-0.388
O2 + γR ⇌ CH2O + OH + propene1ol	1×10^{-6}	2×10^{-4}	0.010	reservoir state	0.650	γDoubleβscissionFromα E_0	-0.391

Table S16: Branching ratio uncertainty for γRO2 at 300 K and 1×10^{5} Pa. The median and 90% confidence interval of the branching ratio for each pathway are shown using data from Monte carlo simulations. For each branch point, the two parameters with the highest correlation, τ, determined using the Spearman rank correlation, are shown with their corresponding values. See S2 for description of the parameter names.

path	5%	50%	95%	factor	τ	factor	τ
γQOOHα ⇌ γRO2	0.024	0.975	1.000	γ-αQOOHIsom E_0	-0.502	γH2OForm E_0	0.379
γRO2 ⇌ H2O + γaldoxy	1×10^{-6}	0.002	0.643	γH2OForm E_0	-0.700	γQOOHαE_0	0.507
γQOOHγ ⇌ γRO2	1×10^{-7}	4×10^{-4}	0.673	γ-αQOOHIsom E_0	0.614	γ-γQOOHIsom E_0	-0.513
γQOOHβ ⇌ γRO2	1×10^{-10}	6×10^{-6}	0.077	γ-βQOOHIsom E_0	-0.561	imaginary freq. γ-βQOOHIsom	0.511
O2 + γR ⇌ γRO2	1×10^{-12}	2×10^{-7}	0.013	$r_{\gamma R+O_2}$	0.653	γR E_0	-0.532

Table S17: Branching ratio uncertainty for γRO2 at 600 K and 3×10^{5} Pa. The median and 90% confidence interval of the branching ratio for each pathway are shown using data from Monte carlo simulations. For each branch point, the two parameters with the highest correlation, τ, determined using the Spearman rank correlation, are shown with their corresponding values. See S2 for description of the parameter names.

path	5%	50%	95%	factor	τ	factor	τ
O2 + γR ⇌ γRO2	2×10^{-5}	0.179	0.995	$r_{\gamma R+O_2}$	0.849	γR E_0	-0.359
γRO2 ⇌ H2O + γaldoxy	1×10^{-4}	0.077	0.946	reservoir state	0.481	$r_{\gamma R+O_2}$	-0.421
γQOOHα ⇌ γRO2	5×10^{-6}	0.065	0.931	γQOOHαE_0	-0.447	reservoir state	-0.441
γQOOHγ ⇌ γRO2	1×10^{-7}	0.001	0.315	γQOOHγE_0	-0.495	reservoir state	-0.461
γRO2 ⇌ OH + disub_c4ether	7×10^{-6}	0.003	0.261	γC4EtherFromα E_0	-0.569	reservoir state	0.387
γRO2 ⇌ OH + disub_epoxy	2×10^{-6}	6×10^{-4}	0.065	γ-βQOOHIsom E_0	-0.646	$r_{\gamma R+O_2}$	-0.406
γRO2 ⇌ HO2 + γalkene	2×10^{-6}	9×10^{-4}	0.052	γHO2elimFromRO2 E_0	-0.533	$r_{\gamma R+O_2}$	-0.479
γRO2 ⇌ CH2O + ipropylOOH	5×10^{-6}	7×10^{-4}	0.031	$r_{\gamma R+O_2}$	-0.509	γ-αQOOHIsom E_0	0.399

Table S18: Branching ratio uncertainty for γRO2 at 900 K and 1×10^{6} Pa. The median and 90% confidence interval of the branching ratio for each pathway are shown using data from Monte carlo simulations. For each branch point, the two parameters with the highest correlation, τ, determined using the Spearman rank correlation, are shown with their corresponding values. See S2 for description of the parameter names.

path	5%	50%	95%	factor	τ	factor	τ
O2 + γR ⇌ γRO2	6×10^{-4}	0.764	0.999	$r_{\gamma R+O_2}$	0.914	γR E_0	-0.270
γRO2 ⇌ H2O + γaldoxy	6×10^{-5}	0.029	0.739	$r_{\gamma R+O_2}$	-0.661	reservoir state	0.454
γQOOHα ⇌ γRO2	1×10^{-9}	2×10^{-4}	0.534	reservoir state	-0.657	γQOOHαE_0	-0.402
γRO2 ⇌ OH + disub_c4ether	1×10^{-5}	0.007	0.366	$r_{\gamma R+O_2}$	-0.659	reservoir state	0.379
γRO2 ⇌ HO2 + γalkene	5×10^{-6}	0.008	0.220	$r_{\gamma R+O_2}$	-0.800	γHO2elimFromRO2 E_0	-0.362
γQOOHγ ⇌ γRO2	2×10^{-10}	1×10^{-5}	0.183	reservoir state	-0.689	γQOOHγE_0	-0.404
γRO2 ⇌ OH + disub_epoxy	2×10^{-6}	0.002	0.104	$r_{\gamma R+O_2}$	-0.742	γ-βQOOHIsom E_0	-0.461
γRO2 ⇌ CH2O + ipropylOOH	6×10^{-6}	0.002	0.055	$r_{\gamma R+O_2}$	-0.786	γAlkoxyIsom E_0	-0.346
γRO2 ⇌ OH + γaldol	3×10^{-7}	3×10^{-4}	0.021	$r_{\gamma R+O_2}$	-0.680	γAldolFromα E_0	-0.431
γRO2 ⇌ CH2O + OH + propene1ol	1×10^{-7}	2×10^{-4}	0.016	$r_{\gamma R+O_2}$	-0.696	γDoubleβscissionFromα E_0	-0.399
γRO2 ⇌ CH2O + OH + propene3ol	4×10^{-8}	1×10^{-4}	0.014	$r_{\gamma R+O_2}$	-0.694	reservoir state	0.420

Table S19: Overall rate uncertainty at 300 K and 1×10^{5} Pa. The median and 90% confidence interval of the branching ratio for each reaction are shown using data from Monte carlo simulations. For each path, the two parameters with the highest correlation, τ, determined using the Spearman rank correlation, are shown with their corresponding values. See S2 for description of the parameter names.

path	5%	50%	95%	factor	τ	factor	τ
O2 + aR ⟶ products	2.3×10^{10}	6.2×10^{10}	3.1×10^{10}	$r_{\alpha R+O_2}$	1.000	αR $\langle E_{down}\rangle$ exp	0.079
O2 + bR ⟶ products	2.2×10^{11}	2.3×10^{7}	8.0×10^{12}	$r_{\beta R+O_2}$	0.999	imaginary freq. βH2OForm	-0.068
O2 + gR ⟶ products	1.1×10^{13}	3.6×10^{10}	1.6×10^{10}	$r_{\gamma R+O_2}$	1.000	γDoubleβscissionFromγ E_0	-0.096
aRO2 ⟶ products	6.0×10^{4}	730	2×10^{5}	αRO2 E_0	0.721	αAdductFromRO2 E_0	-0.597
bRO2 ⟶ products	6×10^{-8}	0.002	2×10^{-4}	βRO2 E_0	0.778	β-αQOOHIsom E_0	-0.334
gRO2 ⟶ products	0.057	1×10^{-5}	0.065	γRO2 E_0	0.746	γ-αQOOHIsom E_0	-0.566

Table S20: Overall rate uncertainty at 600 K and 3×10^{5} Pa. The median and 90% confidence interval of the branching ratio for each reaction are shown using data from Monte carlo simulations. For each path, the two parameters with the highest correlation, τ, determined using the Spearman rank correlation, are shown with their corresponding values. See S2 for description of the parameter names.

path	5%	50%	95%	factor	τ	factor	τ
O2 + aR ⟶ products	1.1×10^{10}	3.0×10^{10}	1.6×10^{10}	$r_{\alpha R+O_2}$	0.999	αR $\langle E_{down}\rangle$ exp	0.079
O2 + bR ⟶ products	1.0×10^{11}	2.0×10^{7}	5.9×10^{11}	$r_{\beta R+O_2}$	0.986	βRO2 E_0	-0.075
O2 + gR ⟶ products	1.4×10^{12}	1.0×10^{10}	4.5×10^{9}	$r_{\gamma R+O_2}$	0.991	γDoubleβscissionFromγ E_0	-0.096
aRO2 ⟶ products	6.4×10^{7}	4.9×10^{7}	7.6×10^{8}	αRO2 E_0	0.438	αAdductFromRO2 E_0	-0.409
bRO2 ⟶ products	2.5×10^{3}	2×10^{4}	3.3×10^{5}	βRO2 E_0	0.639	$r_{\beta R+O_2}$	0.542
gRO2 ⟶ products	3.5×10^{6}	7.0×10^{3}	1.0×10^{4}	γRO2 E_0	0.719	$r_{\gamma R+O_2}$	0.418

Table S21: Overall rate uncertainty at 900 K and 1×10^6 Pa. The median and 90% confidence interval of the branching ratio for each reaction are shown using data from Monte carlo simulations. For each path, the two parameters with the highest correlation, τ, determined using the Spearman rank correlation, are shown with their corresponding values. See S2 for description of the parameter names.

path	5%	50%	95%	factor	τ	factor	τ
O2 + aR $\longrightarrow$ products	9.1×10^9	2.4×10^{10}	1.3×10^{10}	$r_{\alpha R+O_2}$	0.995	αR E_0	0.082
O2 + bR $\longrightarrow$ products	2.3×10^{10}	1.8×10^7	1.9×10^{10}	$r_{\beta R+O_2}$	0.872	βRO2 E_0	-0.198
O2 + gR $\longrightarrow$ products	1.9×10^{11}	2.2×10^9	6.3×10^8	$r_{\gamma R+O_2}$	0.895	reservoir state	-0.167
aRO2 $\longrightarrow$ products	2.4×10^7	2.1×10^9	1.0×10^{10}	reservoir state	-0.613	αRO2 E_0	-0.309
bRO2 $\longrightarrow$ products	2.5×10^7	1.4×10^7	1.7×10^8	$r_{\beta R+O_2}$	0.694	βRO2 E_0	0.362
gRO2 $\longrightarrow$ products	3.8×10^9	1.8×10^7	8.8×10^6	$r_{\gamma R+O_2}$	0.649	γRO2 E_0	0.349

S3 IRC diagrams

This section shows IRC diagrams for all the reactions in the paper. To view properly, you need a pdf viewer with javascript capabilities, like Adobe Reader. Click on an image to view the IRC calculation.

S3.1 α-network

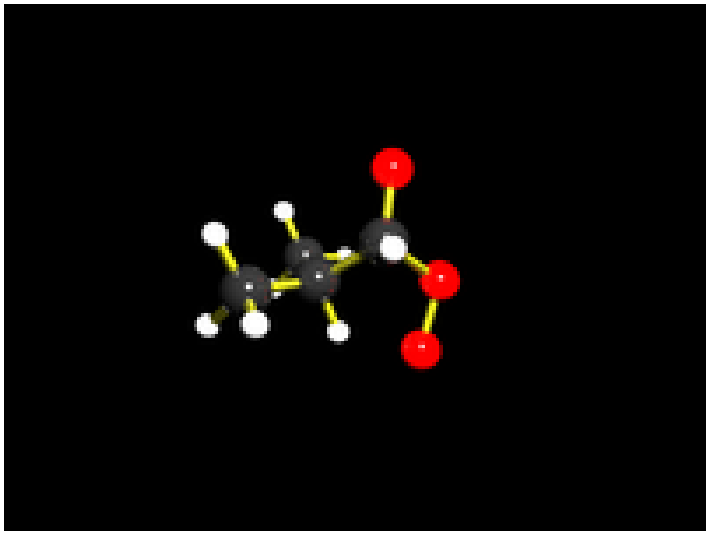

Figure S4: Some of the IRC steps for α-βQOOHIsom

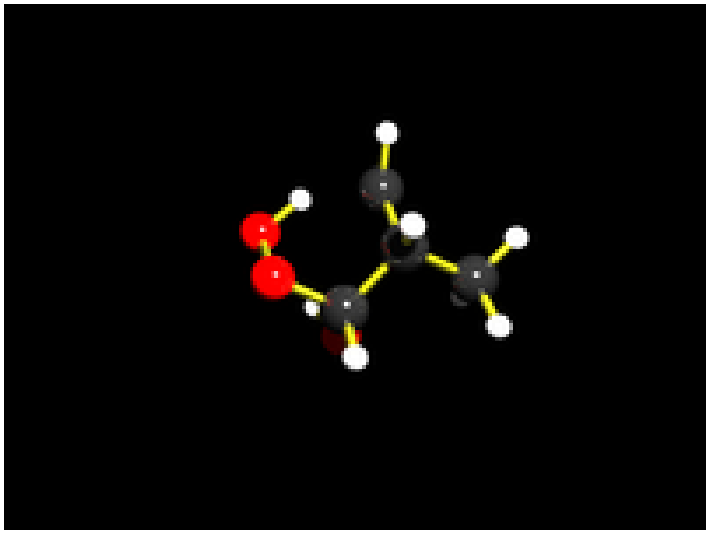

Figure S5: Some of the IRC steps for α-γQOOHIsom

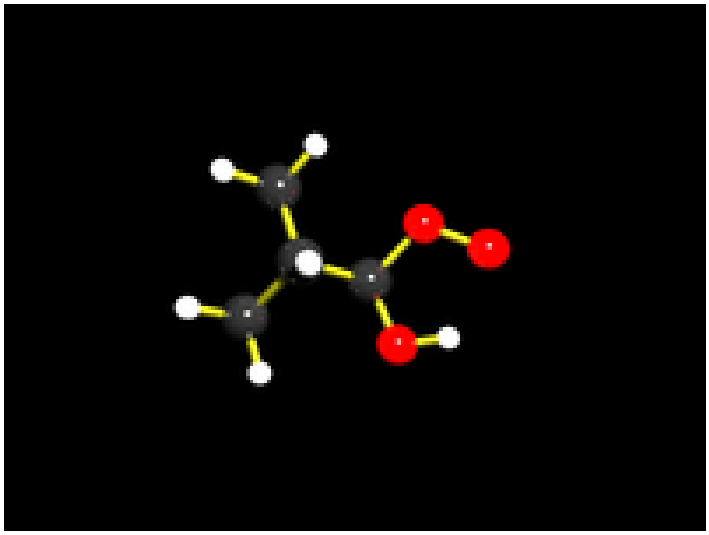

Figure S6: Some of the IRC steps for αAlkoxyIsom

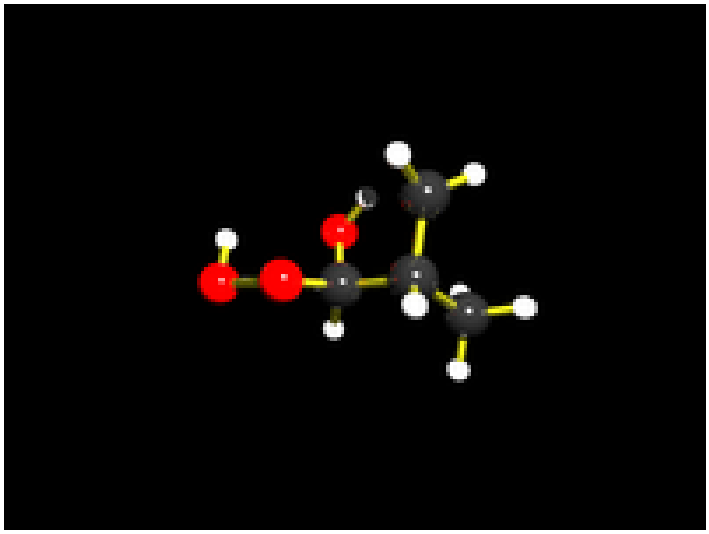

Figure S7: Some of the IRC steps for αAlkoxyIsomFromγ

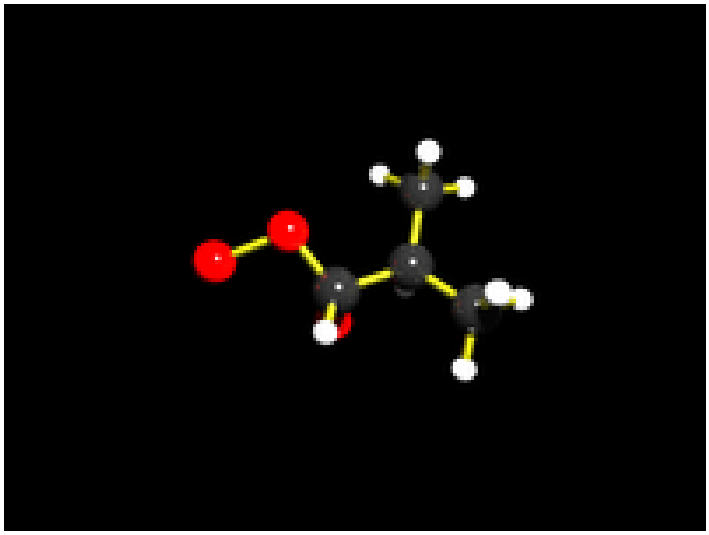

Figure S8: Some of the IRC steps for αAlkoxyIsomFromγ

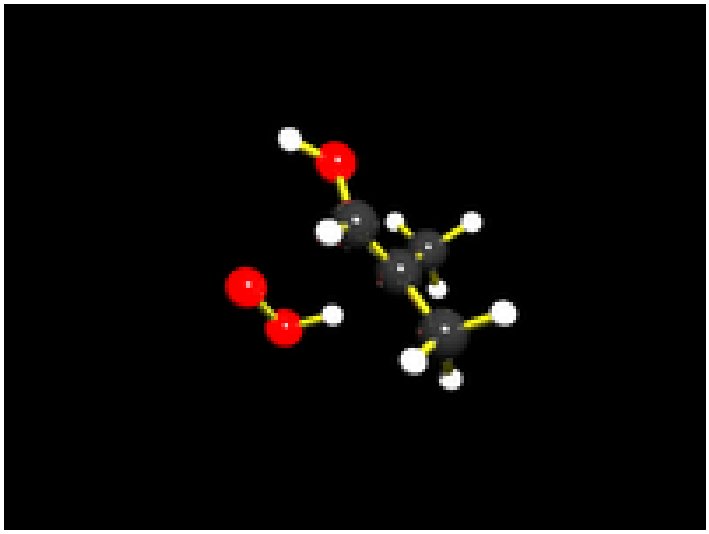

Figure S9: Some of the IRC steps for αHO2elimFromRO2

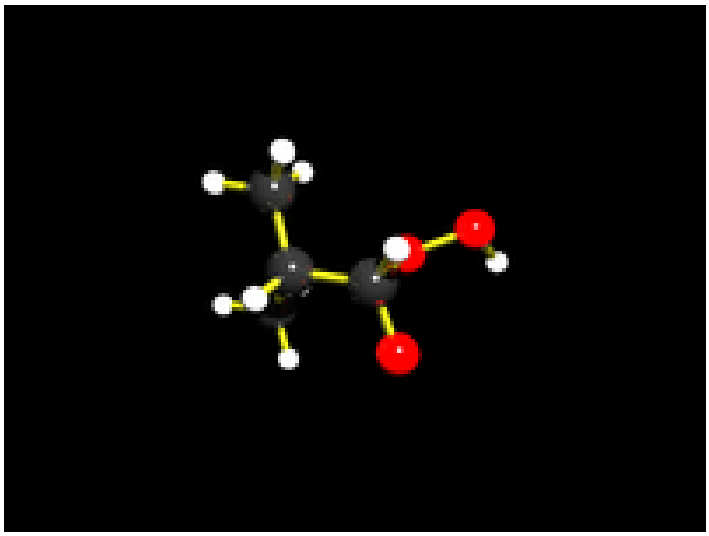

Figure S10: Some of the IRC steps for αHO2elimFromAlkoxy

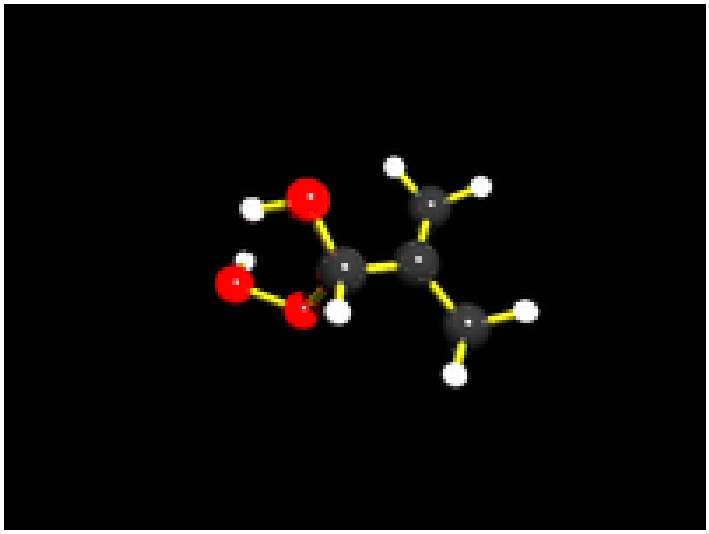

Figure S11: Some of the IRC steps for αHO2elimFromβ

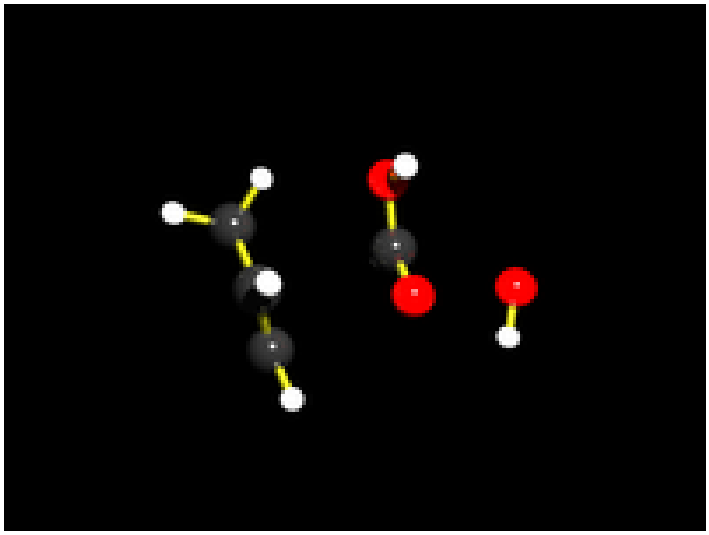

Figure S12: Some of the IRC steps for αDoubleβscission

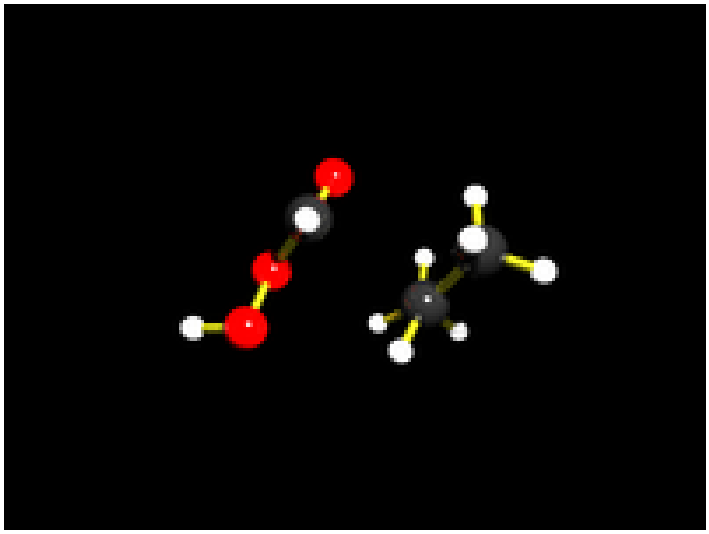

Figure S13: Some of the IRC steps for α-βscissionFromAlkoxy

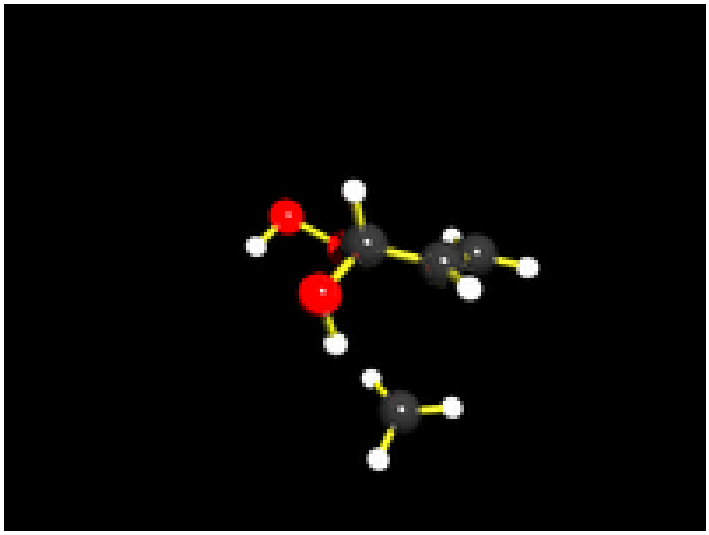

Figure S14: Some of the IRC steps for α-βscissionFromγ

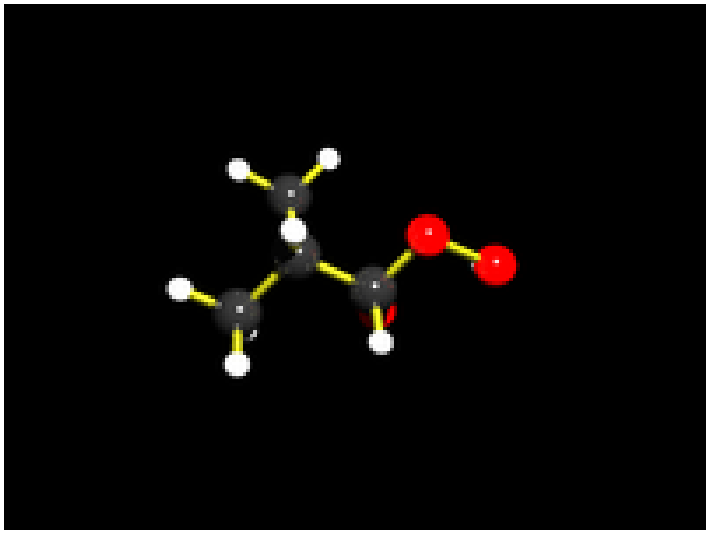

Figure S15: Some of the IRC steps for αHejection

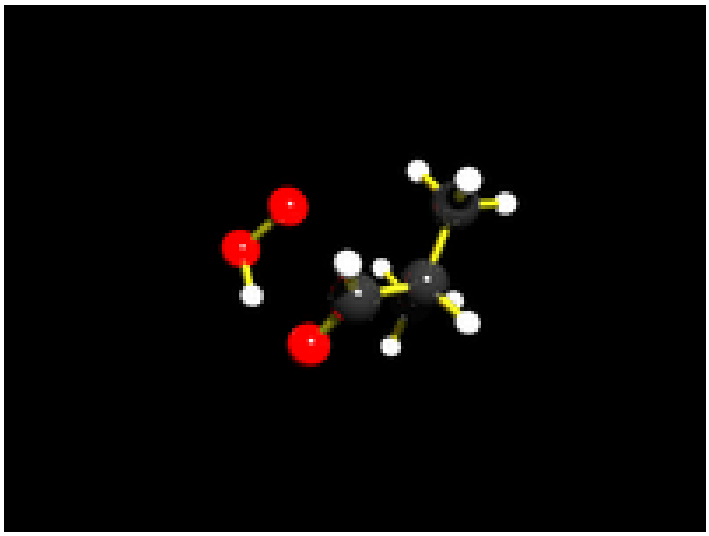

Figure S16: Some of the IRC steps for αAdductFromRO2

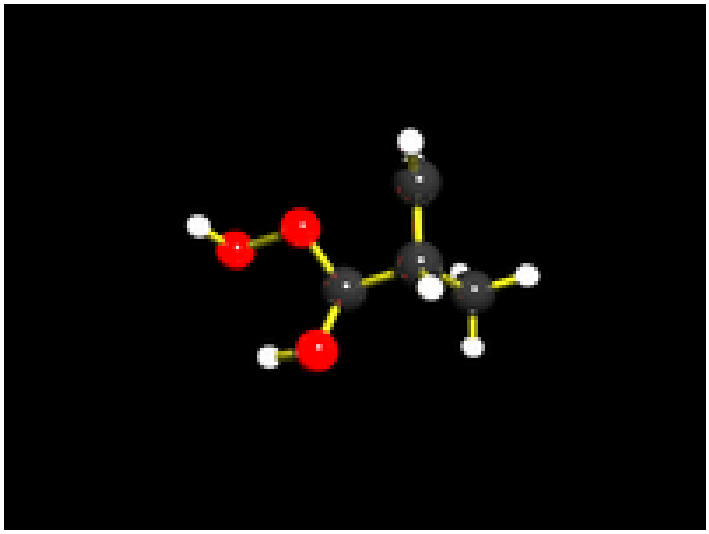

Figure S17: Some of the IRC steps for αC4EtherFromγ

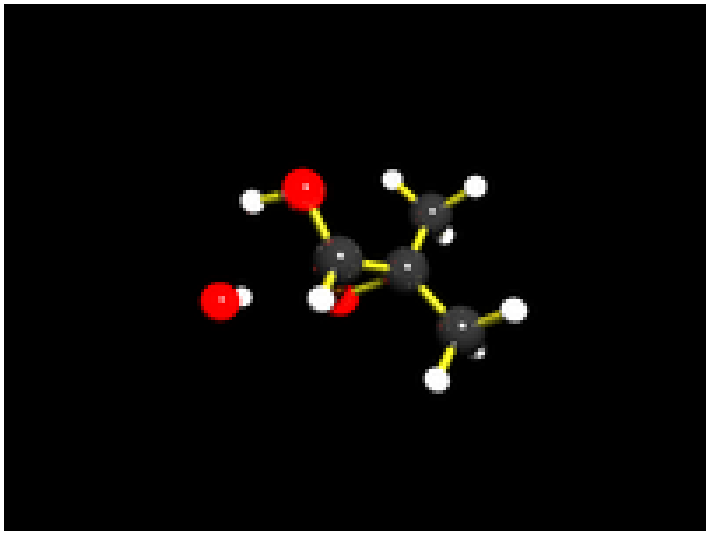

Figure S18: Some of the IRC steps for αEpoxyFromβ

S3.2 β-network

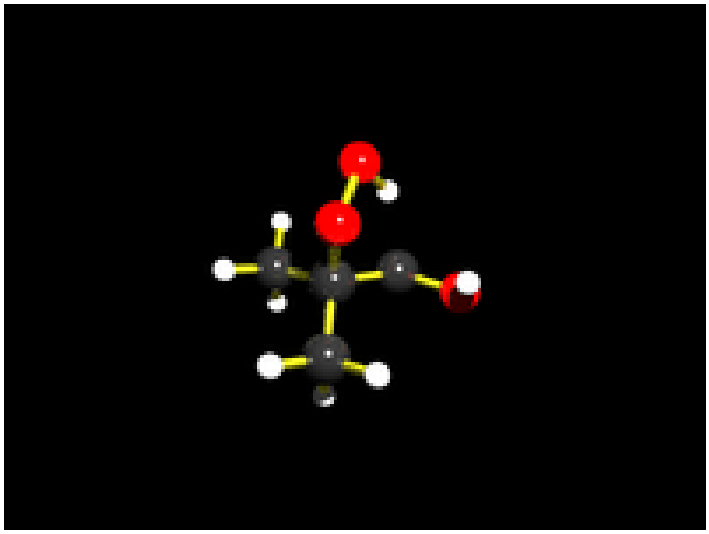

Figure S19: Some of the IRC steps for β-αQOOHIsom

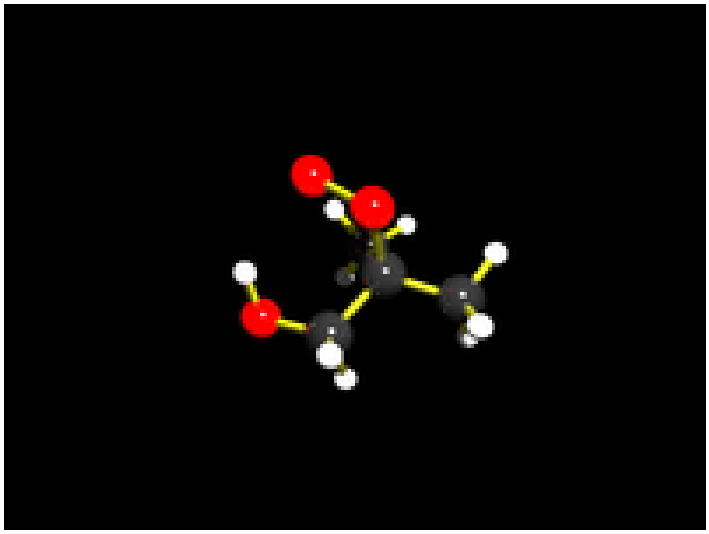

Figure S20: Some of the IRC steps for β-γQOOHIsom

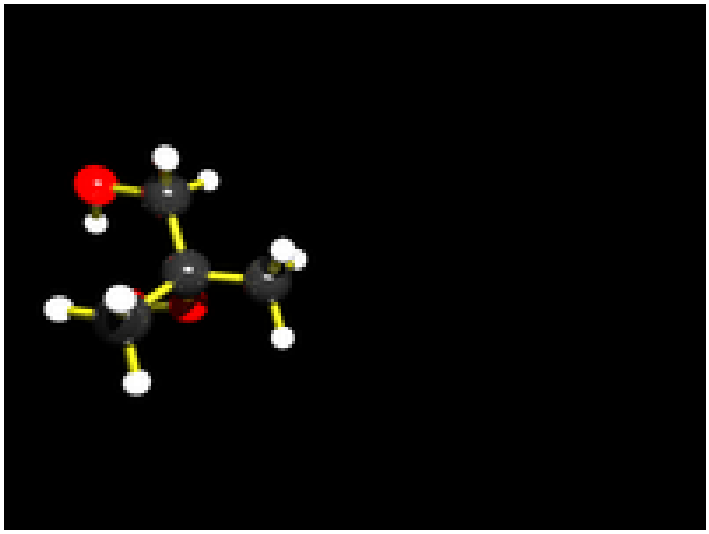

Figure S21: Some of the IRC steps for βAlkoxyIsom

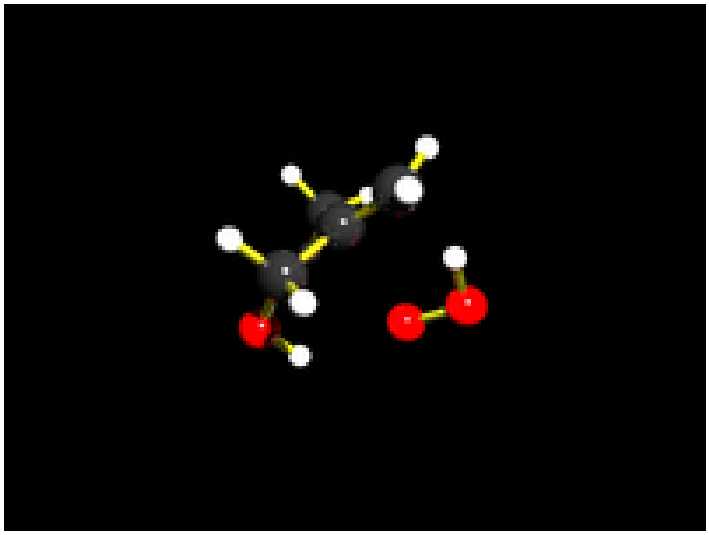

Figure S22: Some of the IRC steps for β-γHO2elimFromRO2

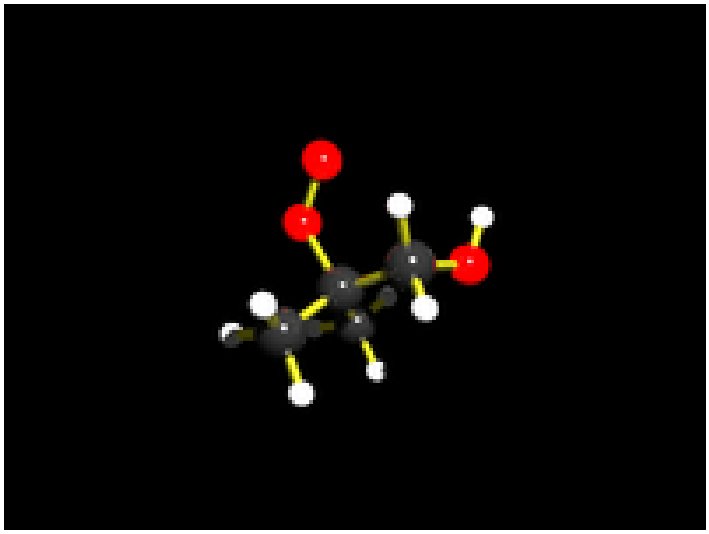

Figure S23: Some of the IRC steps for β-αHO2elimFromRO2

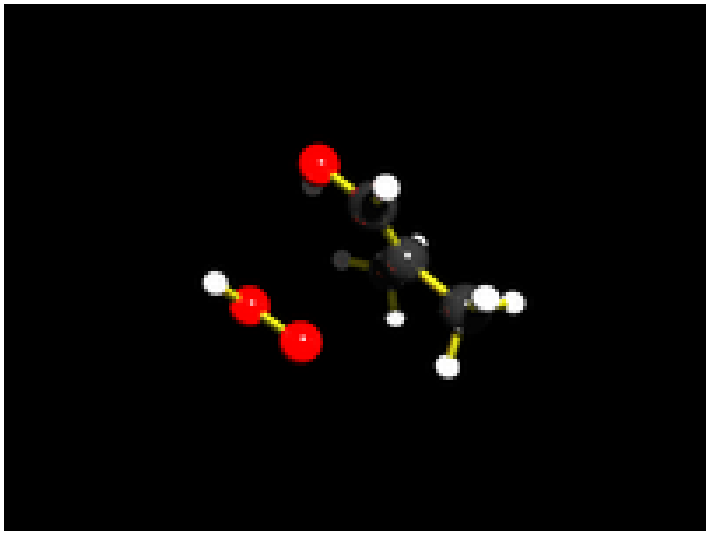

Figure S24: Some of the IRC steps for βHO2elimFromα

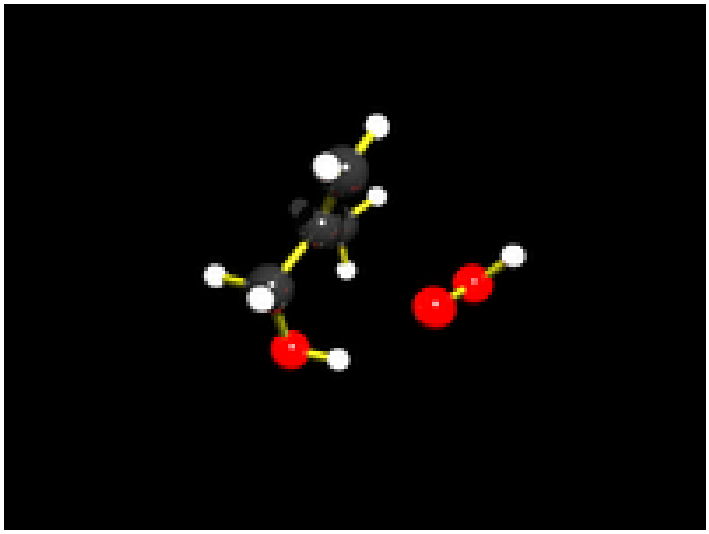

Figure S25: Some of the IRC steps for βHO2elimFromγ

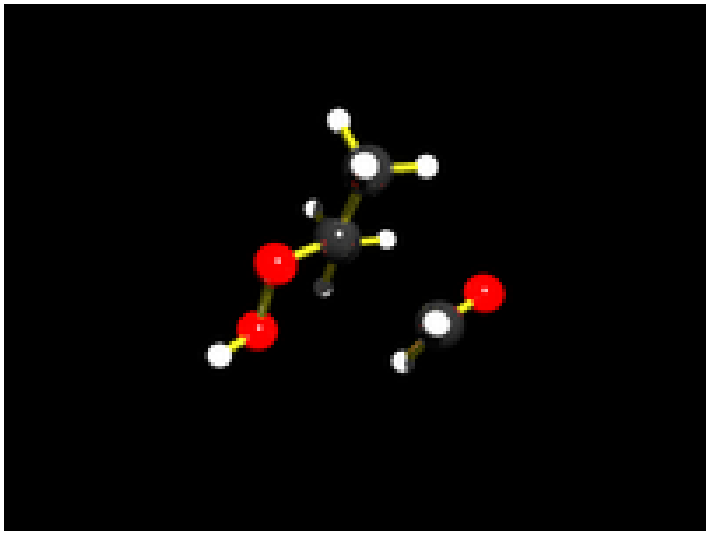

Figure S26: Some of the IRC steps for β-βscissionFromAlkoxy

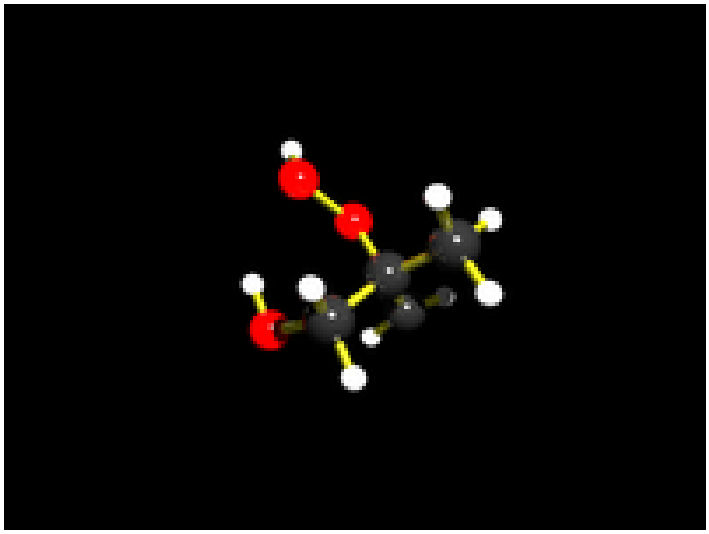

Figure S27: Some of the IRC steps for βEpoxyFromγ

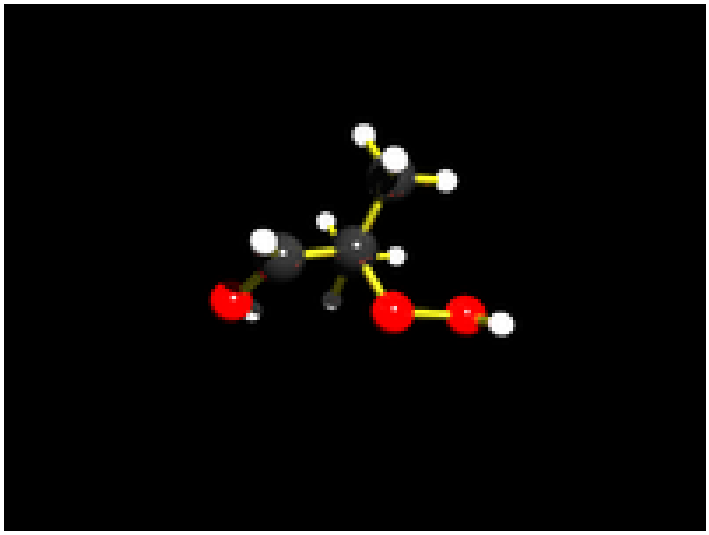

Figure S28: Some of the IRC steps for βEpoxyFromα

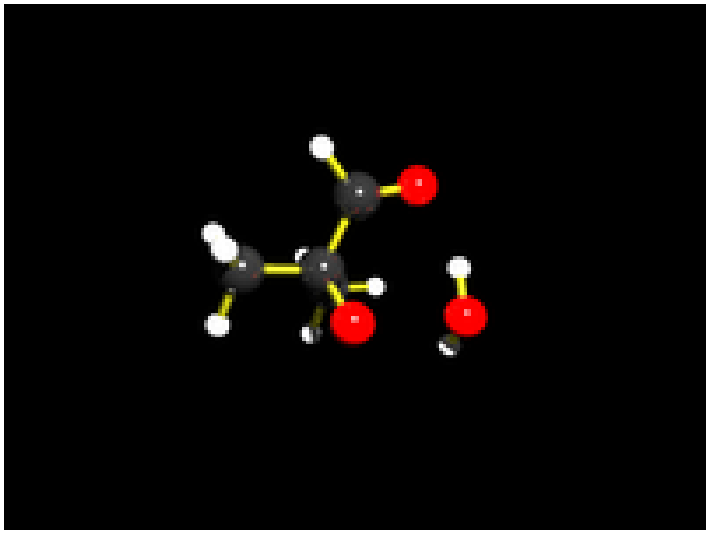

Figure S29: Some of the IRC steps for βH2OForm

S3.3 γ-network

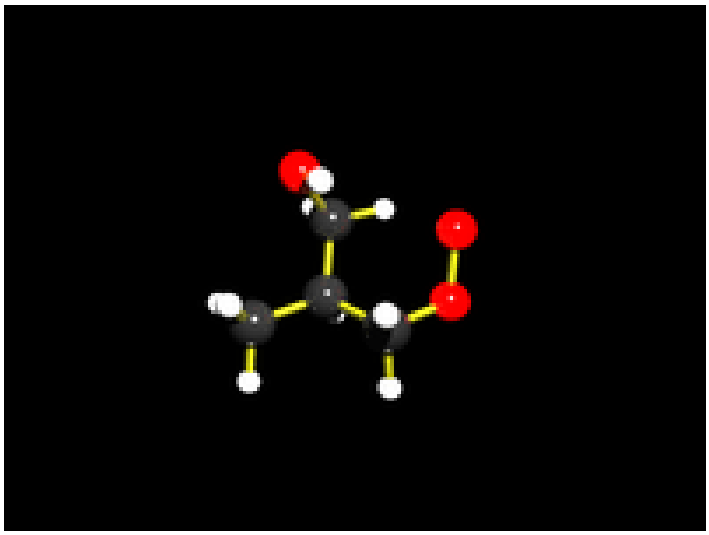

Figure S30: Some of the IRC steps for γ-αQOOHIsom

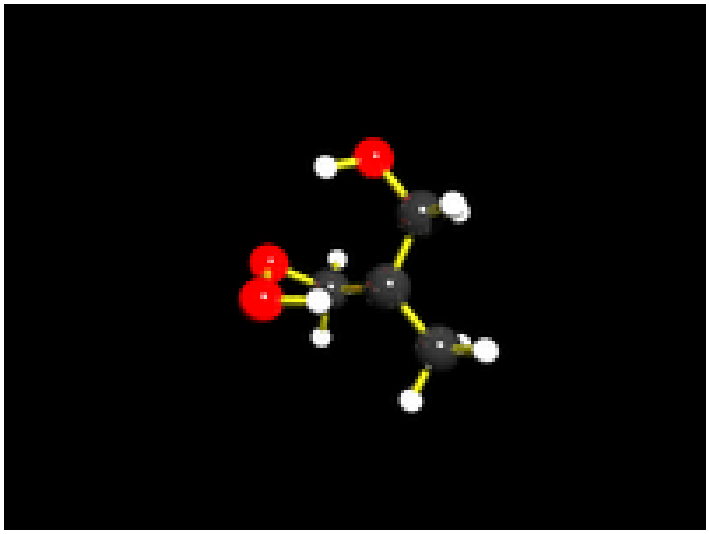

Figure S31: Some of the IRC steps for γ-βQOOHIsom

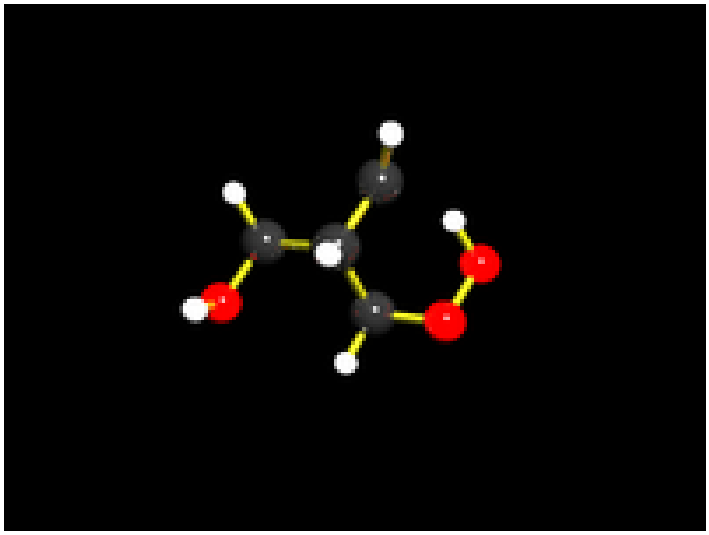

Figure S32: Some of the IRC steps for γ-γQOOHIsom

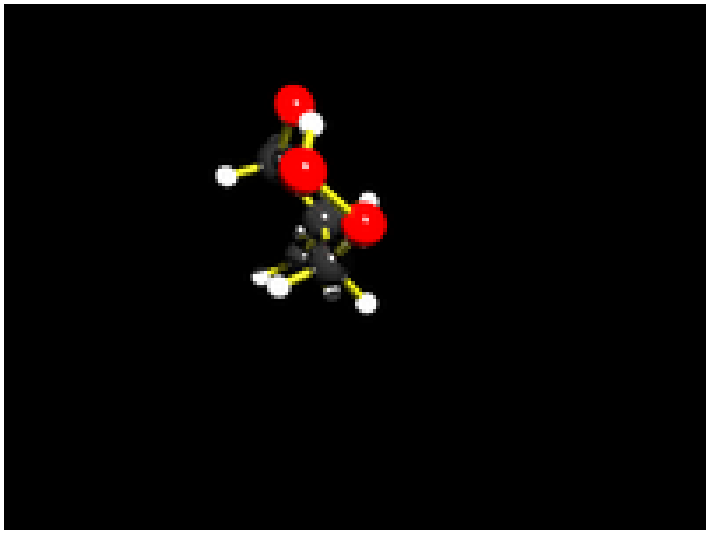

Figure S33: Some of the IRC steps for γAlkoxyIsom

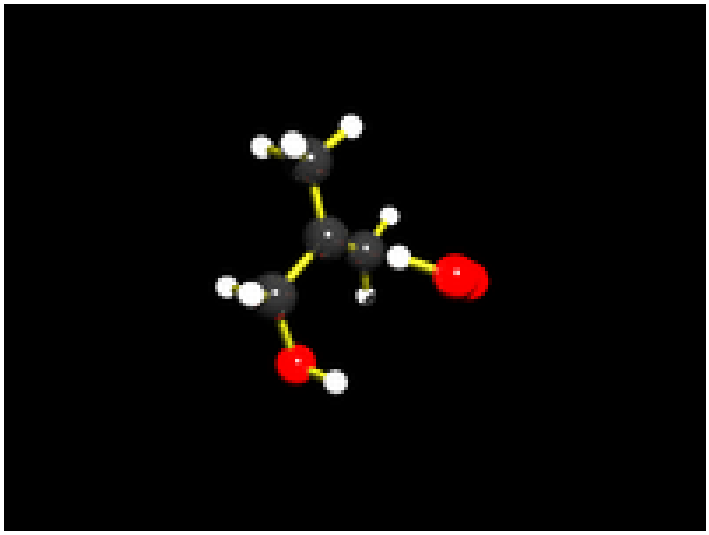

Figure S34: Some of the IRC steps for γHO2elimFromRO2

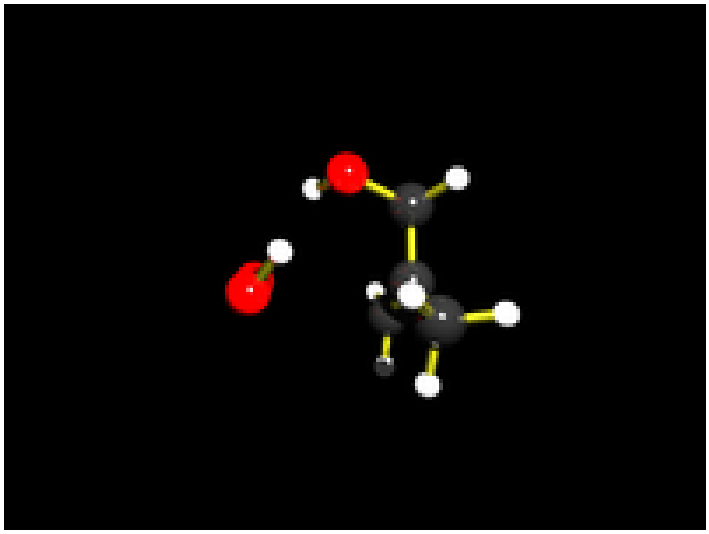

Figure S35: Some of the IRC steps for γHO2elimFromβ

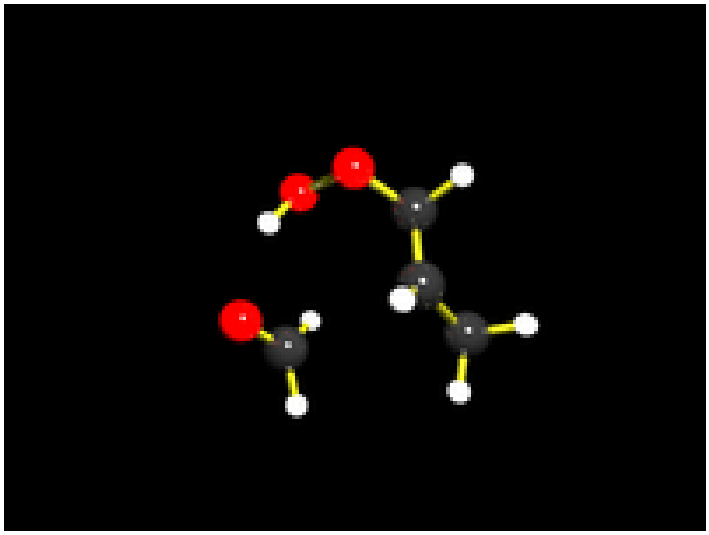

Figure S36: Some of the IRC steps for γ-βscissionFromAlkoxy

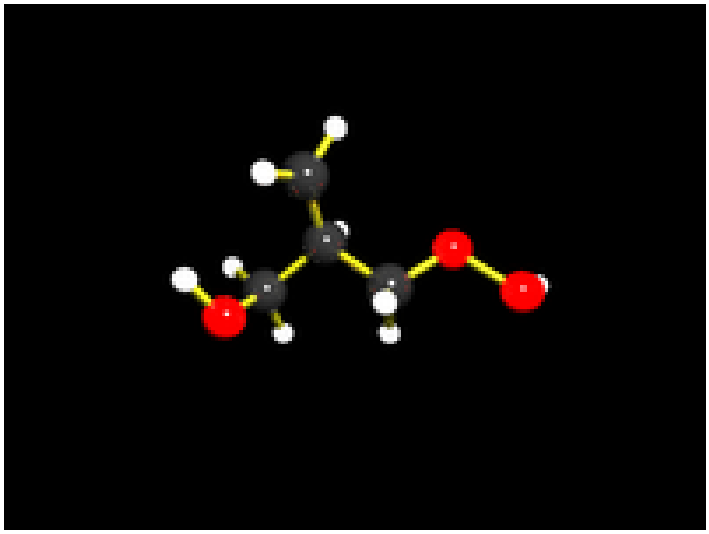

Figure S37: Some of the IRC steps for γDoubleβscissionFromγ

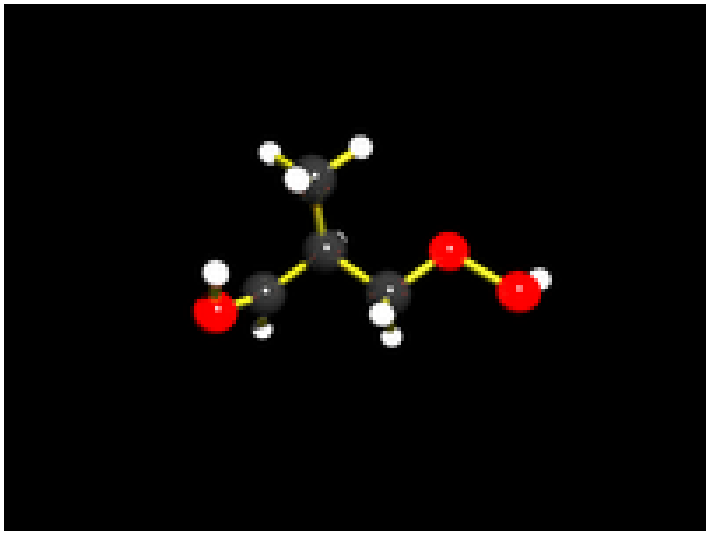

Figure S38: Some of the IRC steps for γDoubleβscissionFromα

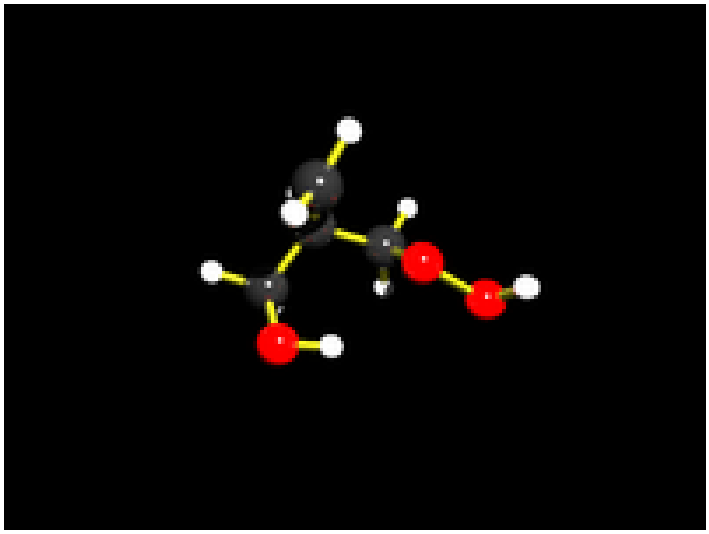

Figure S39: Some of the IRC steps for γC4EtherFromγ

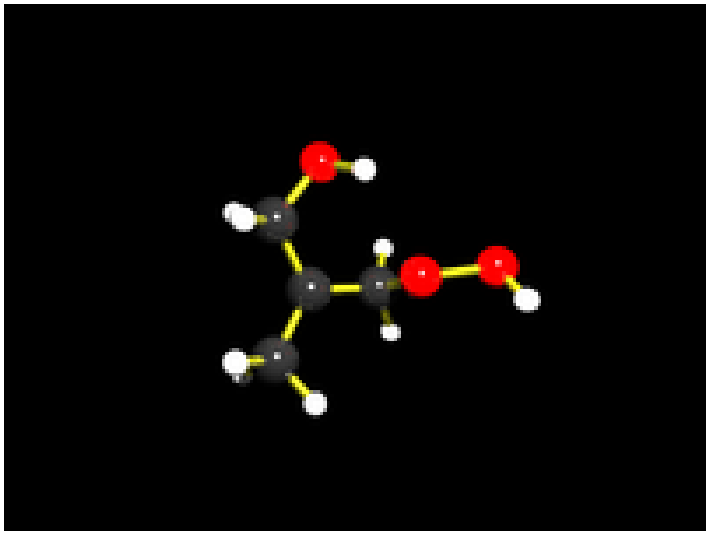

Figure S40: Some of the IRC steps for γEpoxyFromβ

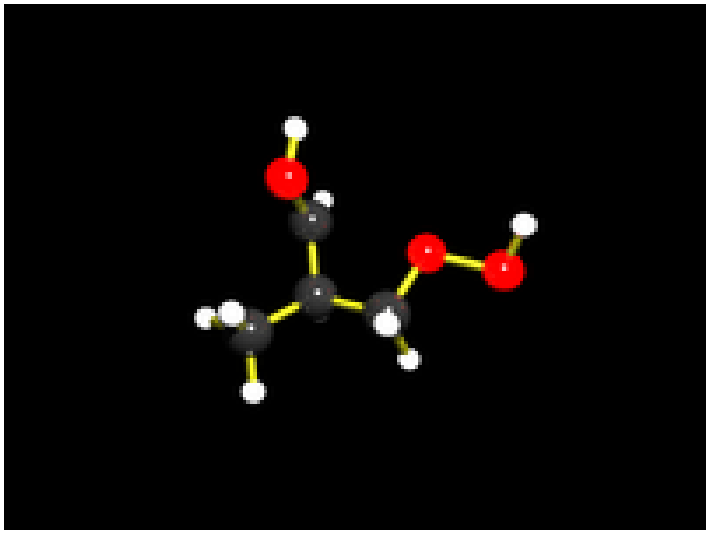

Figure S41: Some of the IRC steps for γC4EtherFromα

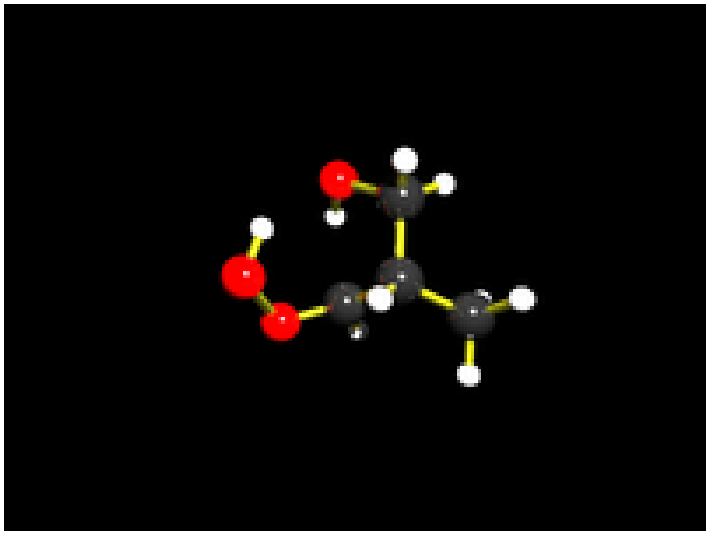

Figure S42: Some of the IRC steps for γAlkoxyHabs

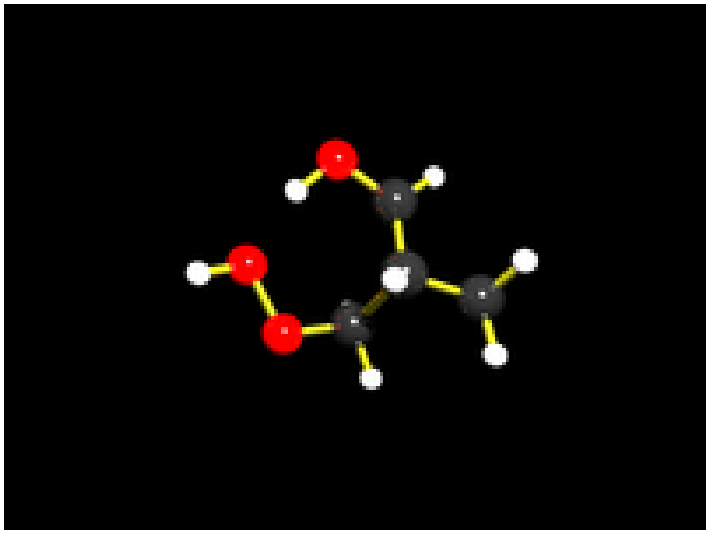

Figure S43: Some of the IRC steps for γH2OForm

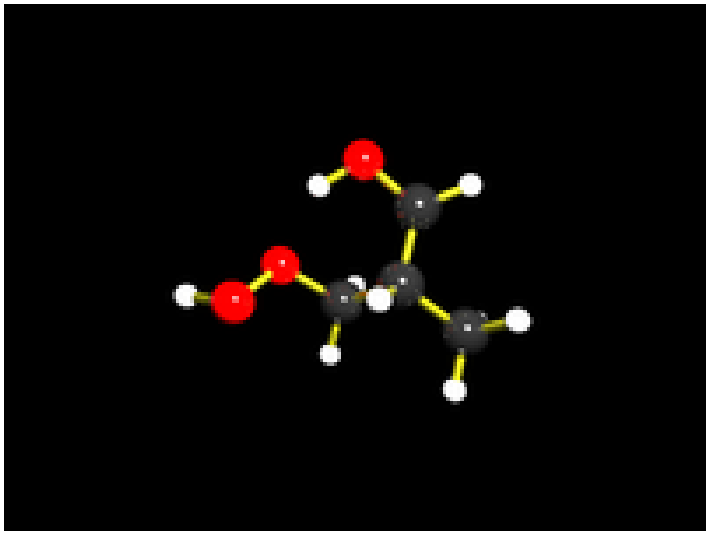

Figure S44: Some of the IRC steps for γAdolFromα

S4 Other Figures

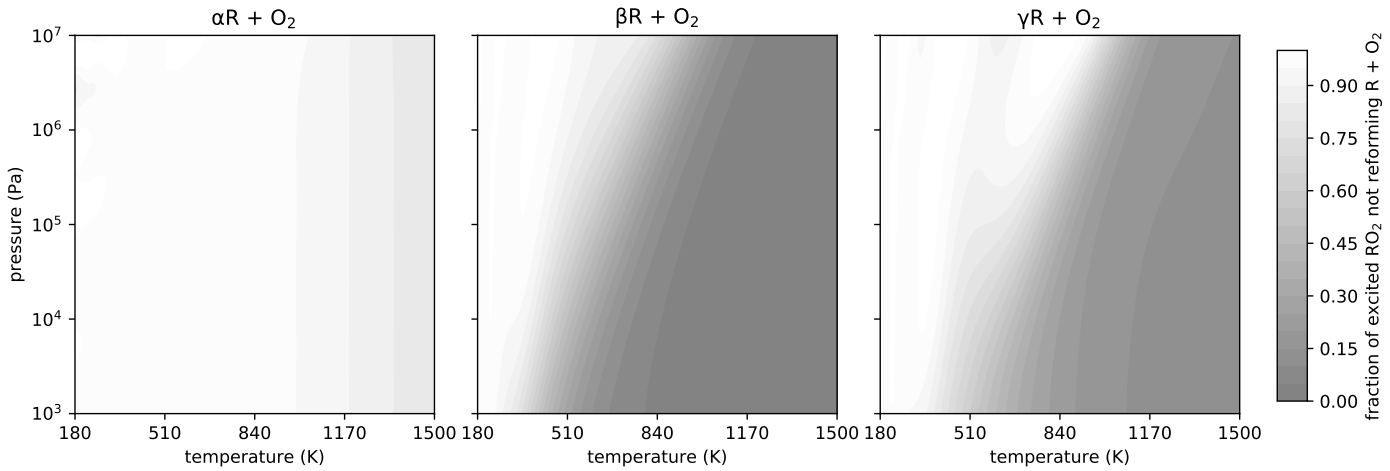

Figure S45: The fraction of excited RO_2 that go back to form $R + O_2$ for the three surfaces at various temperatures and pressures. Periodic behavior at lower temperatures and high fractions of reaction are likely artifacts created from the sum of all the fitted pressure-dependent rates not perfectly fitting to the high-pressure-limit Arrhenius rate.